buildings

MDPI

Article

Experimental Characterization of Composite Bamboo Shear Wall Panels Under Monotonic and Cyclic Loading

Mary Joanne C. Aniñon [1], Mees C. Fabel [2], Lessandro Estelito O. Garciano [1,*], Luis Felipe Lopez [3] and Nischal P. N. Pradhan [3]

[1] Department of Civil Engineering, Gokongwei College of Engineering, De La Salle University, Manila 1004, Philippines; mary_joanne_aninon@dlsu.edu.ph
[2] Department of Civil and Environmental Engineering, Technological University Eindhoven, P.O. Box 513 Eindhoven, The Netherlands; m.c.fabel@student.tue.nl
[3] Base Bahay Foundation, Inc., Makati 1231, Philippines; luis.lopez@base-bahay.com (L.F.L.); nischal.pradhan@base-bahay.com (N.P.N.P.)
* Correspondence: lessandro.garciano@dlsu.edu.ph

Abstract

The escalating global demand for sustainable and disaster-resilient housing has renewed interest in bamboo-based construction systems, particularly composite bamboo shear wall (CBSW) panels as low-carbon alternatives to conventional materials. Despite their potential, systematic data on the shear performance of such panels remains limited, especially regarding the influence of cross-bracing on strength, stiffness, ductility, dissipated energy, and damage behavior under lateral loading. This study addresses this gap through experimental characterization of full-scale CBSW panels. Two configurations, with (WT1) and without (WT2) flat steel bar cross-bracing, were tested under monotonic and cyclic loading. WT1 panels consistently exhibited a higher characteristic shear strength and capacity, and initial stiffness than WT2. WT2 panels showed greater ductility through more distributed deformation. Both configurations displayed gradual strength deterioration post-peak. The Energy Equivalent Elastic–Plastic (EEEP) method yielded higher and more conservative estimates of yield load and displacement compared to the conventional approach. These findings demonstrate that CBSW panels, particularly WT1, offer viable lateral resistance for low-rise structures in seismic-prone regions.

Keywords: bamboo; bamboo structures; shear wall; lateral loading performance; composite bamboo shear wall

Academic Editor: Deuckhang Lee

Received: 16 March 2026
Revised: 2 April 2026
Accepted: 9 April 2026
Published: 14 April 2026

1. Introduction

The growing global housing demand, intensified by rapid urbanization and population growth, continues to widen the housing gap, particularly in developing countries [1,2]. At the same time, the worsening impacts of climate change emphasize the need for sustainable, low-carbon, and resilient construction materials. Timber has long been a preferred material for housing due to its strength-to-weight ratio and renewability [3]. However, the slow growth of timber limits its availability for large-scale housing production.

Bamboo presents a promising alternative to timber. Bamboo possesses a high strength-to-weight ratio, making it an ideal material for structural load-bearing applications [4,5]. Furthermore, it is a rapidly renewable resource that matures significantly faster than timber, allowing it to become available for structural applications much sooner [6,7].

Native bamboo is primarily distributed across Asia, America, and Africa. Although no species are native to Europe, many have been successfully introduced and cultivated across the continent [8]. This widespread availability ensures the material remains accessible in regions where housing shortages are most severe. Despite these advantages, its significant natural variability in geometry and mechanical properties brings challenges in construction. Ultimately, the use of bamboo in permanent structures remains limited due to an overwhelming lack of knowledge and experimental data [9].

This study investigates a hybrid structural system known as the composite bamboo shear wall (CBSW) [10], which has been successfully implemented in the construction of thousands of houses in recent years [11]. This system is a modern adaptation of the traditional *bahareque* [10] of Latin America, where timber or bamboo frames are sheathed with woven bamboo or timber strips and/or plastered with earthen materials [12–14]. Similarly, the *tabique pampango* [15] in the Philippines adopted a comparable construction method. The proposed CBSW integrates bamboo culms and timber framing, which may include steel bracings, together with a mortar cladding system that enhances durability, dimensional stability, and heat resistance [10]. The timber plates address the irregularity of bamboo culms by providing a leveled and uniform frame connection, while the mortar cladding serves as protective reinforcement against environmental exposure and thermal effects. This composite configuration offers a sustainable and practical solution for low-rise buildings, particularly in bamboo-rich regions.

CBSW panels are analogous to those of conventional light-frame timber (LFT) shear walls. In timber buildings, LFT shear walls serve as the primary lateral force-resisting system under horizontal loads induced by wind or earthquakes. Over the past two decades, the in-plane performance of LFT shear walls has been extensively investigated through both monotonic and cyclic testing. For instance, Manser et al. [16] experimentally evaluated the shear resistance of timber-framed walls sheathed with oriented strand board (OSB), while Branco et al. [17] conducted a comprehensive series of monotonic and cyclic tests to characterize the in-plane behavior of light timber wall panels with various cladding materials. Similarly, Xiao et al. [18] examined the lateral loading response of lightweight wood-frame shear walls incorporating ply-bamboo sheathing, systematically varying parameters such as wall dimensions, nail types, nail quantities, and nail spacing. More recently, Gangi et al. [3] assessed the seismic performance of modern bamboo lightweight shear walls constructed with glued laminated bamboo (glubam) frames, with particular emphasis on the energy dissipation provided by cladding-to-framing connections.

Collectively, these studies have established a robust experimental and analytical foundation for understanding the load-carrying mechanism, particularly the dominant role of cladding-to-framing connections, in lightweight shear wall systems. In a bamboo-based structural system, shear walls similarly serve as the primary elements resisting lateral loads induced by wind and earthquakes. Recent studies have begun to explore analogous composite configurations. Kou et al. [9] evaluated the cyclic behavior of bamboo frame walls with gypsum-based mortar cladding, while Villalba-Morales et al. [19] examined the seismic response of *bahareque* walls under in-plane horizontal loading, demonstrating the promising potential of bamboo-mortar composites. Kaminski et al. [10] significantly advanced this field by collating and analyzing preliminary strengths, stiffness, and ductility from various CBSW studies across Costa Rica, Colombia, Mexico, London, and Coventry. Nevertheless, a clear research gap persists with respect to CBSW panels intended for permanent low-rise structures, particularly those incorporating cement-based mortar cladding, where systematic experimental data under monotonic and cyclic loading remain limited. This scarcity of comprehensive performance characterization hinders the development of reliable design guidance and limits the confident application of such systems in seismic-prone regions.

https://doi.org/10.3390/buildings16081540

A specific and underexplored aspect is the role of cross-bracings in CBSW performance. In the initial CBSW design, flat steel bar cross-bracing is typically included to improve load distribution, reduce localized demands on nailed connections, and increase overall strength and stiffness—attributes particularly valuable in seismic-prone regions. However, the use of steel bracing introduces additional cost and embodied carbon, prompting the question of whether equivalent performance can be achieved without it. Unbraced configurations rely more heavily on the nailed cladding–frame interaction, which may allow greater deformability and ductility through more distributed damage but risks earlier strength degradation. Comparing braced and unbraced configurations is, therefore, essential to quantify trade-offs in strength, stiffness, ductility, dissipated energy, and failure modes. While this study focuses on the individual performance of braced and unbraced panels, the results could inform future design flexibility. Selectively omitting bracing in certain panels with a multi-panel structure or mixing braced and unbraced configurations based on local demand offers a potential strategy to balance structural performance with cost and environmental impact.

The novelty of this research is centered on two primary advancements. First, it presents the development of a modern, standardized bamboo–mortar composite shear wall system, transitioning the technology from traditional practice to an engineered, code-compliant structural solution. Second, this study provides the first systematic, full-scale experimental investigation using the ISO 21581:2010 (E) Method I [20] protocol to formally evaluate the structural performance of CBSW systems under monotonic and cyclic loading.

This study addresses the identified gaps through an experimental investigation of full-scale CBSW panels integrating bamboo culms, timber plates, optional steel bracing, and reinforced mortar cladding. For each configuration, a preliminary monotonic loading test was performed on an individual specimen primarily to calibrate the protocol used for the subsequent series of reversed cyclic tests. By characterizing shear behavior under monotonic and cyclic loading, the work generates essential performance data to support evidence-based design of CBSW structures. In particular, the comparison of braced and unbraced configurations provides critical insight into trade-offs that could guide future optimization, reducing reliance on steel while preserving structural reliability. Ultimately, the findings aim to strengthen the technical foundation for CBSW systems and advance their adoption as safe, sustainable, and resilient solutions for low-rise housing in seismic-prone regions.

2. Materials and Methods

2.1. Materials

Bambusa blumeana bamboo was used as vertical studs in the wall frames. The bamboo culms were harvested at an age of 3 to 5 years, with outer diameters ranging from 80 to 100 mm and wall thicknesses between 8 and 20 mm. Prior to use, the culms were chemically treated with a permethrin solution or a Borax and Boric Acid (BBA) mixture to enhance durability and resistance to insect and fungal attacks. Material consistency was ensured by sourcing treated bamboo culms from treatment facilities—the Kanya Kawayan Treatment Facility in Batangas and the Kawayan Collective in Tarlac, Philippines—that follow established grading procedures in accordance with ISO 19624:2018 [21]. This standard-based grading served as the primary mechanism to manage natural variability by enforcing strict limits on geometric irregularities and visual defects. Refer to [22] for detailed mechanical properties of *Bambusa blumeana* bamboo.

Kiln-dried spruce pine fir timber was used as top and bottom plates of the frames. Each member had nominal dimensions of 88 mm (width), 38 mm (thickness), and 2400 mm (length), with all four sides smoothly finished (S4S).

https://doi.org/10.3390/buildings16081540

Metal reinforcements, including flat steel bars (referred to as flat bar in this study), deformed reinforcing steel bars (referred to as embedded rebar in this study), and threaded rods, were used to connect the members of the frame. The flat bars conformed to BS 4360:1990 Grade 43A [23], with a nominal tensile strength of 410 MPa and dimensions of 25 mm (width) and 3 mm (thickness). The 12 mm diameter embedded rebars conformed to ASTM A615/A615M-22 Grade 40 [24] and have a minimum tensile strength of 420 MPa. The threaded rods, with diameters of 10 mm and 12 mm, complied with ASTM A307-21 Grade A [25] and have a nominal tensile strength of 414 MPa.

The wall matrix was composed of expanded metal lath, commonly known as rib lath. The rib lath was manufactured from hot-dip galvanized sheet steel with a thickness ranging from 0.3 to 0.5 mm, conforming to ASTM A653/A653M-20 [26]. Each steel had a width of 610 mm and a length of 2440 mm.

Cement mortar was used for two applications, as infill and as plaster, in accordance with ASTM C1329/C1329M-12 [27]. The mix proportion was 1 part Portland cement Type I to 3 parts fine aggregate by volume. The water–cement ratio was 0.9 for mortar infill and 0.5 for mortar plaster. Both mortar types were tested at 7 days following the ASTM C109/C109M-21 [28]. The average compressive strength was 21.88 $\pm$ 8.71 MPa for mortar plaster and 19.68 $\pm$ 8.71 MPa for mortar infill.

Common nails with gauge numbers 12 and 10 were used for connections, conforming to ASTM F1667/F1667M-21a [29]. The gauge number 12 nails have a nominal diameter of 2.5 mm and a nominal length of 38 mm, while the gauge number 10 nails have a nominal diameter of 3.3 mm and a nominal length of 64 mm. The nominal tensile strength for both nail types is 435 MPa.

2.2. Specification of Wall Panels

Two composite bamboo shear wall (CSBW) panel configurations were considered in this study, designated as WT1 and WT2. Each wall panel consisted of three main components: (a) framing, (b) cladding, and (c) cladding-to-framing nailed connections. Both wall types have an aspect ratio of 1:1, with overall dimensions of 2.4 m $\times$ 2.4 m.

Figure 1 illustrates the WT1 configuration. The WT1 panel comprises 5 vertical bamboo studs (B1–B5), a timber top plate (TP1), a timber bottom plate (TP2), and flat bar cross-bracing (FB1 and FB2). The WT2 panel has the same framing layout and dimensions as WT1 but without the flat bar cross-bracing (FB1 and FB2). The assembly of the CBSW panel involves seven specific connection types: (i) nailed connections between bamboo studs and timber plates, (ii) J-bolt connections for top-end anchoring, (iii) embedded rebar connections for bottom-end anchoring, (iv) bolt connections between flat bar and timber plates, (v) bolt connections between flat bar and bamboo studs, (vi) nailed connections between rib lath and timber plates, and (vii) nailed connections between rib lath and bamboo studs. These connection types are illustrated in Figure 2 and are described in detail in the following paragraph.

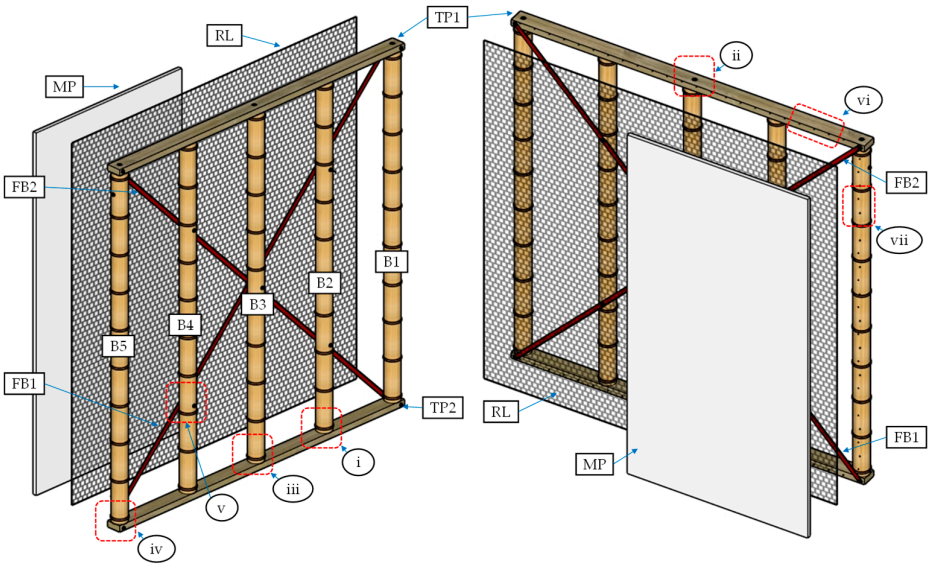

(**a**) (**b**)

Figure 1. Components of the CBSW panel showing (**a**) the rear elevation and (**b**) the front elevation in isometric view.

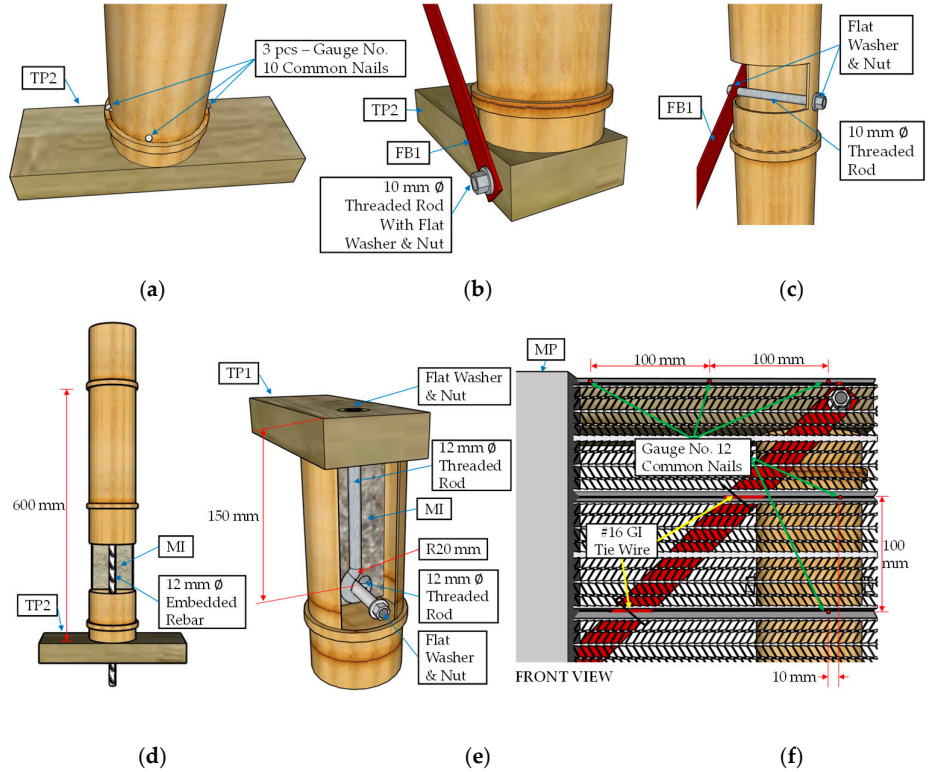

(**d**) (**e**) (**f**)

Figure 2. Various connections in the CBSW panel: (**a**) nailed connection between bamboo studs and timber plates; (**b**) bolt connection between flat bar and timber plates; (**c**) bolt connection between flat bar and bamboo studs; (**d**) embedded rebar connection; (**e**) J-bolt connection; (**f**) nailed connection between rib lath and framing components, and GI tie wire connection.

Several types of connections were used to assemble the framing system, as shown in Figure 2. The first type was a nailed connection (i), consisting of three pieces of gauge no. 10 common nails, which fastened all bamboo studs (B1–B5) to the timber plates (TP1 and

TP2), as shown in Figure 2a. The second type was a J-bolt connection (ii), fabricated from 12 mm diameter threaded rods bent into a J-shape, anchoring the bamboo studs (B1, B3, and B5) to the top timber plate (TP1). The uppermost internode of each bamboo stud containing the J-bolt was filled with mortar infill (MI) to provide anchorage, as illustrated in Figure 2e. The third type was an embedded rebar connection (iii), where 12 mm diameter reinforcing bars were inserted into two internodes of the bamboo studs (B1, B3, and B5) and filled with mortar infill (MI) to provide anchorage to the bottom timber plate (TP2) and foundation, as demonstrated in Figure 2d. The flat bar cross-bracing (FB1 and FB2), when installed, was bolted (iv) to the timber plates (TP1 and TP2) at their ends using 10 mm diameter threaded rods, as presented in Figure 2b. Each bracing was also connected to the intermediate bamboo studs (B2–B4) through the same type of bolted connection (v), as demonstrated in Figure 2c.

Two distinct nailing patterns were employed to connect the rib lath to the framing, as illustrated in Figure 2f. First (vi), on the timber plates (TP1 and TP2), gauge no. 12 common nails were placed at 100 mm center-to-center spacing along the horizontal direction. Second (vii), on the vertical bamboo studs (B1–B5), gauge no. 12 common nails were arranged in a staggered (zigzag) configuration, with 100 mm vertical spacing and 10 mm horizontal spacing. This staggered nailing pattern was intended to prevent premature splitting of the bamboo studs under lateral forces.

The assembly of the wall framing integrates these components and connection types. All bamboo studs (B1–B5) were attached to the top and bottom timber plates (TP1 and TP2) using nailed connections (i). In addition, bamboo studs B1, B3, and B5 were anchored to the top timber plate (TP1) with J-bolt connections (ii) and to the bottom timber plate (TP2) and foundation with embedded rebar connections (iii). The flat bar cross-bracing (FB1 and FB2), when installed, was bolted to the timber plates (TP1 and TP2) at their ends (iv) and to the intermediate studs (B2–B4) in designated areas (v), as shown in Figure 1.

The cladding system of the wall panel consists of two primary components: the rib lath matrix (RB) and the mortar plaster (MP). The rib lath acted as the base reinforcement for the plaster layer, while the mortar plaster provided the finished surface and protective layer, limiting moisture penetration from rain and thereby safeguarding the internal bamboo and timber elements from weathering.

The rib lath matrix was installed horizontally with a 100 mm overlap between adjacent sheets to ensure continuity. It was nailed to the top and bottom timber plates (TP1 and TP2) using connection (vi) and to the bamboo studs (B1–B5) using connection (vii), as shown in Figure 2f.

In addition to the nailed connection, #16 galvanized iron (GI) tie wire (Standard Wire Gauge) attachments were utilized, as illustrated in Figure 2f. The rib lath matrix was secured to the flat bar cross-bracing (TP1 and TP2) using #16 GI tie wires spaced at 100 mm vertically. Similarly, overlapping portions of rib lath sheets were tied together using #16 GI tie wires at 100 mm horizontal spacing.

Once fixed, the rib lath matrix was coated on one side with mortar plaster (MP), applied in two layers with a nominal total thickness of 25 mm. The second coat was applied at least 10 h after the first to promote adequate curing and bond strength.

2.3. Test Setup

There is currently no established standard specifically for testing composite bamboo shear wall (CBSW) panels. Therefore, ISO 21581:2010 (E) [20], which provides a procedure for testing timber shear walls, was adopted as the reference standard in this study. This standard defines two types of boundary conditions: Method I and Method II. Method I aims to determine the full shear capacity of the wall panel using tie-down rods (or hold-down connectors) to restrain uplift and overturning under monotonic and cyclic loading.

This setup allows the wall to deform primarily in shear. In contrast, Method II replicates actual field conditions by permitting uplift and overturning, which was performed by [30]. In this study, Method I was adopted as the boundary condition for testing the CBSW panels.

Figure 3 illustrates the experimental setup used to evaluate the shear performance of the wall panels. The wall panels were mounted within a reaction frame, which serves as the primary support structure for both the hydraulic actuator and the wall panel.

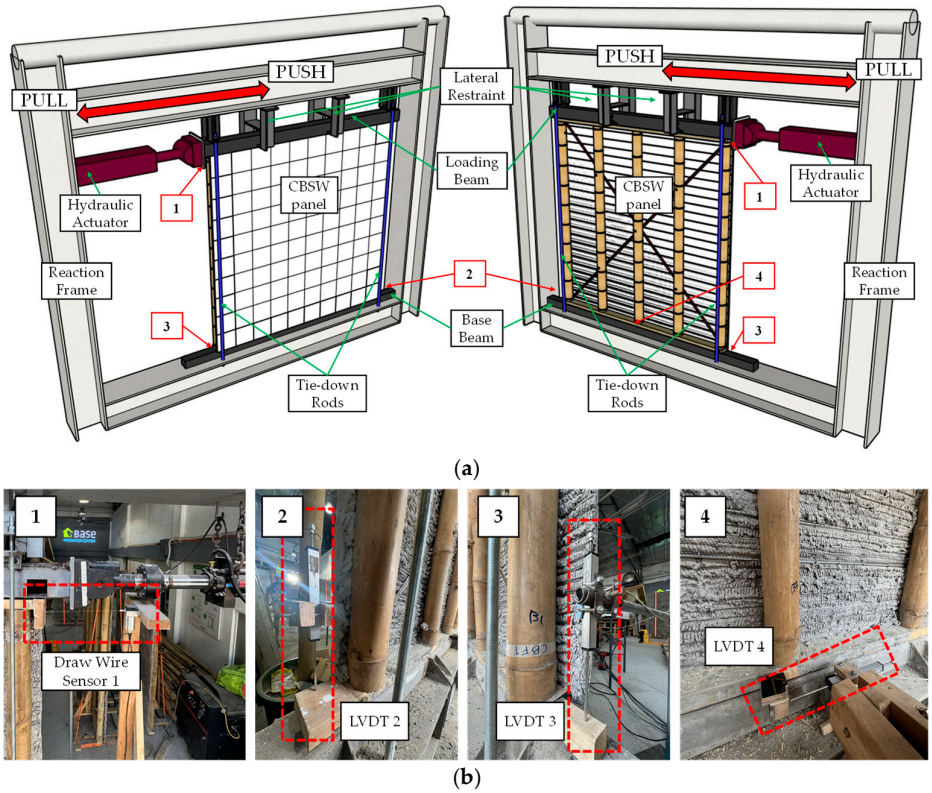

Figure 3. Test setup: (**a**) components of the test setup; (**b**) instrumentations.

A base beam was provided to establish a level foundation for the specimens. It was designed with sufficient stiffness so that its deformation during testing could be considered negligible. The bottom of the wall panel was securely anchored to the base beam using embedded rebars (iii), ensuring resistance against sliding and uplift.

At the top of the specimen, a loading beam was fastened with high-tensile bolts to facilitate uniform transfer of lateral forces. The lateral loading protocol was applied using a hydraulic actuator (MTS Systems Corp., Eden Prairie, MN, USA; sourced via Quantum Technologies Global, Singapore), which was mounted to the loading beam. Lateral restraints were installed at the top of the wall panel to prevent out-of-plane displacements. Additionally, a pair of tie-down rods (or hold-down connectors) was provided to resist uplift and overturning while still allowing the wall to develop in-plane shear failure.

Instrumentation was installed to record both lateral and vertical responses during testing. Linear variable differential transformers (LVDTs) and draw-wire sensors were positioned at four points (1–4), as shown in Figure 3. Point (1) measured the overall lateral drift at the top of the wall panel. Points (2) and (3) recorded any overturning displacements induced by the pushing and pulling actions of the hydraulic actuator; however, overturning was minimal due to the effective restraint provided by the tie-down rods. Point (4) monitored the central (in-plane) displacement of the panel to detect any potential

sliding at the base. The net lateral displacement of the wall panel, used for constructing the load–displacement curve, was determined as the difference between the top lateral drift (point (1)) and the central displacement measured at the base level (point (4)), thereby isolating in-plane shear deformation from any base sliding.

2.4. Test Procedure

Two loading protocols were employed in this experimental program: monotonic and cyclic. The primary difference between these protocols lies in the nature of the applied loading, while minor variation exists in instrumentation. The overall test setup, however, remained identical for both procedures.

The ISO standards do not specify the minimum number of specimens required to obtain reliable shear wall performance data. In contrast, other standards, such as ASTM E2126-19 [31], recommend testing 3 to 5 wall specimens for each panel configuration.

This study tested 6 specimens per configuration, with a total of 12 specimens, as shown in Table 1. For each configuration, only 1 specimen was tested under monotonic loading. The data was used to calibrate the loading protocol to test the remaining 5 wall specimens under reversed cyclic loads. Wall specimens are identified using the format WTX-Test-SY, where WT1 and WT2 denote the two distinct wall configurations (Configuration 1 and Configuration 2, respectively), Test indicates the loading type (M for monotonic or C for cyclic), and SY identifies the individual specimen number (S1 to S6 for WT1, S7 to S12 for WT2).

Table 1. Wall panel configurations.

Panel Configuration	Aspect Ratio	Dimension	Framing Components	Number of Wall Specimens	Loading Protocol
WT1	1:1	2.4 m × 2.4 m	Bamboo vertical studs, timber plates, and flat bar cross-bracing	1	Monotonic
				5	Cyclic
WT2	1:1	2.4 m × 2.4 m	Same as WT1 but without the flat bar cross-bracing	1	Monotonic
				5	Cyclic

2.5. Loading Protocols

2.5.1. Monotonic Test

In the monotonic loading procedure, lateral force is applied at a constant displacement-controlled rate, expressed in terms of lateral drift. The loading sequence is divided into three stages, as shown in Figure 4a: Phase 1, the stabilizing cycle; Phase 2, the stiffness cycle; and Phase 3, the strength cycle. A reference force, F_{ref}, from a trial test was used as the estimated maximum lateral resistance of the wall panel. F_{ref} was equal to 35 kN. During the loading and unloading up to $0.4F_{ref}$, the rate of displacement was maintained at 0.04 mm per second.

For load levels exceeding $0.4F_{ref}$, the rate of loading was adjusted relative to the reference displacement V_{ref} so that the total duration of the test ranges between 5 and 30 min. V_{ref} was equal to 90 mm, and the time to failure considered was 10 min; therefore, the rate of loading was 0.15 mm per second.

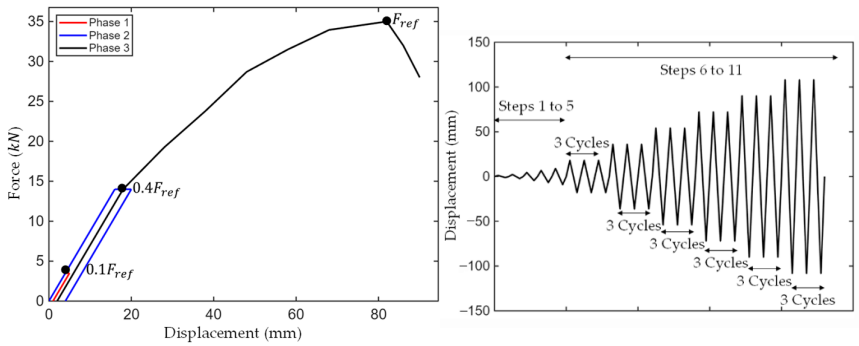

(**a**) (**b**)

Figure 4. Loading protocols: (**a**) monotonic loading; (**b**) cyclic loading.

For the monotonic test, the load was applied by the pulling action of the hydraulic actuator. Three sensors were utilized, as shown in Figure 3a,b: point (1) captured the lateral drift, point (2) measured the overturning displacement, and point (4) recorded the central displacement of the wall panel.

2.5.2. Cyclic Test

The cyclic displacement protocol is illustrated in Figure 4b. Instead of a single monotonic push, the wall was subjected to successive cycles of increasing lateral displacement (drift) demands. The loading sequence begins with single cycles at relatively small amplitudes, which are derived from the ultimate displacement obtained from the monotonic tests. Following these initial steps, the protocol transitioned to sets of 3 fully reversed cycles at higher amplitudes. Each cycle was executed at a constant frequency of 0.1 Hz. The test ended at step 11, which corresponds to the total failure of the wall panels.

The displacement sensors used in the cyclic tests were the same as those employed in the monotonic test. In the cyclic setup, however, an additional sensor was installed at point (3), as illustrated in Figure 3a,b, to capture left-side overturning, since the loading protocol involves bidirectional displacements.

2.6. Structural Performance Parameters

2.6.1. Yield and Ultimate Loads and Displacements

Envelope curves derived from the load–displacement responses were used to determine the maximum shear force (F_{max}) sustained by each wall panel and the corresponding displacement (V_{max}). The ultimate (failure) point was defined as the stage of significant loss of load-carrying capacity after peak strength, with the ultimate force (F_u) taken as 80% of F_{max} if the envelope curve exhibited a gradual post-peak decline. The corresponding displacement (V_u) marked the onset of this limit state, providing a practical indicator of failure suitable for seismic and wind design evaluations.

The yield point represents the transition from elastic to inelastic behavior, where permanent deformation begins due to localized yielding or connection slippage. Accurate identification of this point is essential for calculating ductility and for assessing energy dissipation. Two standardized methods from ISO/TR 21141:2022 [32] were applied to determine the yield point, as illustrated in Figure 5. The first method, adopted from JIS A 1414-2:2010 [33], defines the yield load (F_y) as the intersection of the line connecting the points at $0.1F_{max}$ and $0.4F_{max}$ with a line tangent to the envelope curve and parallel to the segment between $0.4F_{max}$ and $0.9F_{max}$. The corresponding displacement (V_y) is then taken as the displacement corresponding to F_y on the envelope curve. The second method follows the Equivalent Energy Elastic–Plastic (EEEP) procedure in ASTM E2126-19 [31]. In this procedure, the EEEP curve is constructed by equating the area under the

actual envelope curve up to the ultimate displacement (V_u) with the area enclosed by two straight lines: one representing the EEEP stiffness (K_{eeep}) and the other representing the idealized post-yield plastic response (line b). Then, intersection of these two lines defines the equivalent yield displacement ($V_{y,eeep}$), providing an energy-based estimate of the yield point.

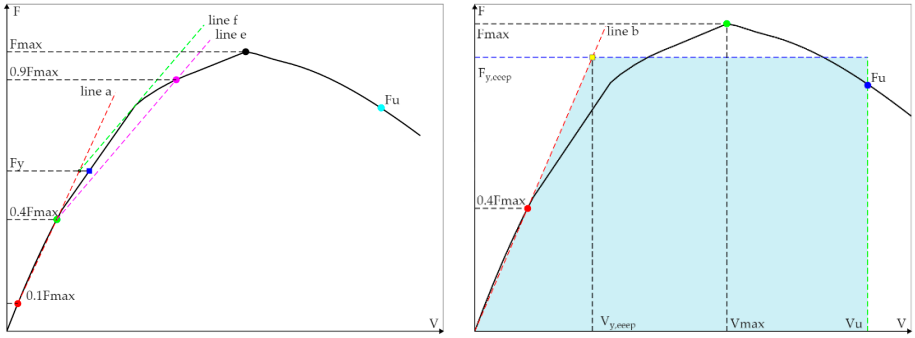

(**a**) (**b**)

Figure 5. Determination of yield points: (**a**) as per JIS A 1414-2:2010 [33] and (**b**) as per ASTM E2126-19 [31].

2.6.2. Lateral Stiffness

For the envelope curve without a distinct linear portion in the elastic range, the elastic stiffness (K_e) can be approximated by the slope of a straight line connecting the points corresponding to 0.1 and 0.4 times the maximum load (F_{max}). Another approach is through the construction of an EEEP curve, as described in the previous section. In this method, the EEEP stiffness (K_{eeep}) is obtained from the slope of a line passing through the origin and the point corresponding to $0.4F_{max}$ on the envelope curve.

2.6.3. Ductility

Ductility is a key performance indicator in structural design as it reflects the capacity of a component to undergo inelastic deformation from yielding to failure without a significant loss of load-bearing capacity. It plays a central role in seismic design, where structures are expected to absorb and dissipate energy through controlled plastic deformation rather than brittle failure. However, its quantification depends on the adopted evaluation criteria and can vary among standards and analytical approaches [34].

The ductility (μ) is defined as the ratio of the ultimate displacement (V_u) to the yield displacement (V_y). For the EEEP approach, the corresponding ductility factor (μ_{eeep}) is the ratio of V_u to the yield displacement derived from the EEEP curve ($V_{y,eeep}$).

2.6.4. Energy Dissipation

Under cyclic loading, the energy dissipated (E_D) in each cycle is quantified as the area enclosed by the hysteresis loop, as illustrated in Figure 6. The cumulative dissipated energy, obtained by summing up the areas of successive hysteresis loops, represents the total energy the wall panel has dissipated up to a given cycle.

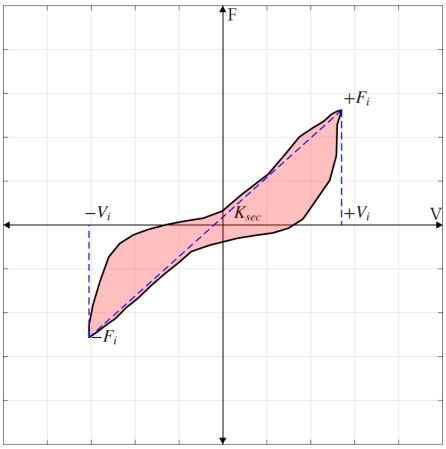

Figure 6. Diagram for computing the equivalent viscous damping ratio.

The equivalent viscous damping ratio (ζ_{eq}) expresses the hysteretic energy dissipation in an equivalent linear–viscous framework and is computed as the ratio of the dissipated energy (E_D) to the maximum strain energy (E_{SO}) stored in the wall at the peak displacements of the same cycle times 4π, as shown in Equations (1) and (2). E_{SO} corresponds to the area of the idealized elastic triangle (blue dashed line and the X-axis) defined by the envelope of the positive and negative peak points, as presented in Figure 6. In this study, ζ_{eq} is evaluated at the third cycle of each loading step.

$$\zeta_{eq} = \frac{1}{4\pi}\left(\frac{E_D}{E_{SO}}\right) \tag{1}$$

$$E_{SO} = \frac{1}{2}KV_i^{\,2} \tag{2}$$

2.6.5. Stiffness Degradation

In this study, the secant stiffness for each cycle was evaluated using Equation (3), which defines stiffness as the ratio of the change in shear force to the corresponding change in lateral displacement between the extreme points of each hysteresis loop. This equation is appropriate for CBSW panels because their load–displacement response becomes nonlinear at very small lateral displacements.

$$K_{sec} = \frac{|+F_i| + |-F_i|}{|+V_i| + |-V_i|} \tag{3}$$

2.7. Characteristic Shear Strength and Shear Capacity

Characteristic strength values for the CBSW panels were determined following the direct evaluation method outlined in ISO 12122-6:2017 [35]. This method accounts for both material variability and statistical uncertainty by calculating the 5th percentile value, providing a 75% confidence level that the actual panel strength exceeds this threshold. Although the standard was originally developed for timber structures and large assemblies, it was adopted here due to the absence of a dedicated standard for CBSW panels.

The procedure starts with the maximum lateral load (F_{max}) recorded in each monotonic and cyclic test. The 5th percentile characteristic strength (f_k) is then obtained by fitting either a normal or a lognormal distribution to the full set of F_{max} values. Distribution choice is guided by the Anderson–Darling and Kolmogorov–Smirnov goodness-of-fit tests.

When the data are consistent with a normal distribution, the characteristic value (f_k) is calculated as:

$$f_k = m\{1 - kV\} \tag{4}$$

where m is the sample mean of all F_{max} values, k is the sampling factor dependent on sample size and assuming unknown population variance, and V is the coefficient of variance computed using Equations (5) and (6).

$$S = \sqrt{\frac{1}{n-1}\sum_{i=1}^{n}\left(F_{max,i} - m\right)^2} \tag{5}$$

$$V = \frac{S}{m} \tag{6}$$

where S is the sample standard deviation.

For lognormally distributed data, the characteristic value (f_k) is calculated as:

$$f_k = exp[m_{ln} - kV_{ln}] \tag{7}$$

where m_{ln} is the sample mean of $\ln\left(F_{max,i}\right)$, k is the sampling factor as above, and V_{ln} is the coefficient of variance derived using Equations (8) and (9).

$$S_{ln} = \sqrt{\frac{1}{n-1}\sum_{i=1}^{n}\left(\ln F_{max,i} - \ln m_{ln}\right)^2} \tag{8}$$

$$V_{ln} = \frac{S_{ln}}{m_{ln}} \tag{9}$$

Because the population variance is unknown (no prior large dataset exists for these specific CBSW configurations), the most conservative sampling factors (k) from ISO 12122-06:2017 [35] are used. These factors provide a statistical adjustment that accounts for the higher uncertainty inherent in small datasets. By applying a larger k value as a penalty for smaller sample sizes, the method ensures that the derived characteristic values maintain the required 75% confidence level. Relevant values for the present sample sizes are given in Table 2.

Table 2. Values for k for 5% characteristic value [35].

n	1	2	3	4	5	6	8	10	11	20	30	∞
V_X	-	-	3.37	2.63	2.33	2.18	2.00	1.92	1.90	1.76	1.73	1.64

The characteristic shear capacity is finally obtained by dividing the characteristic strength values $\boldsymbol{f_k}$ by the nominal wall width (2.4 m).

3. Results and Discussion

3.1. General Response and Damage Modes

The lateral response of the wall panels was evaluated from the load–displacement curves obtained under monotonic and cyclic loading. Figures 7a and 8a show the monotonic load–displacement relationships for WT1 and WT2, respectively, with envelope curves derived according to ISO/TR 21141:2022 [32] to characterize strength deformation behavior. WT1, reinforced with flat bar cross-bracing, exhibited significantly higher lateral strength and initial stiffness than WT2, which lacked bracing. Under monotonic loading, WT1 displayed strain-hardening behavior, with load continuing to increase beyond the yield point before reaching peak strength, indicating the cross-bracing's contribution to post-yield capacity. In contrast, WT2 showed a flatter post-peak response, reflecting reduced stiffness and a diminished ability to sustain resistance after the maximum load.

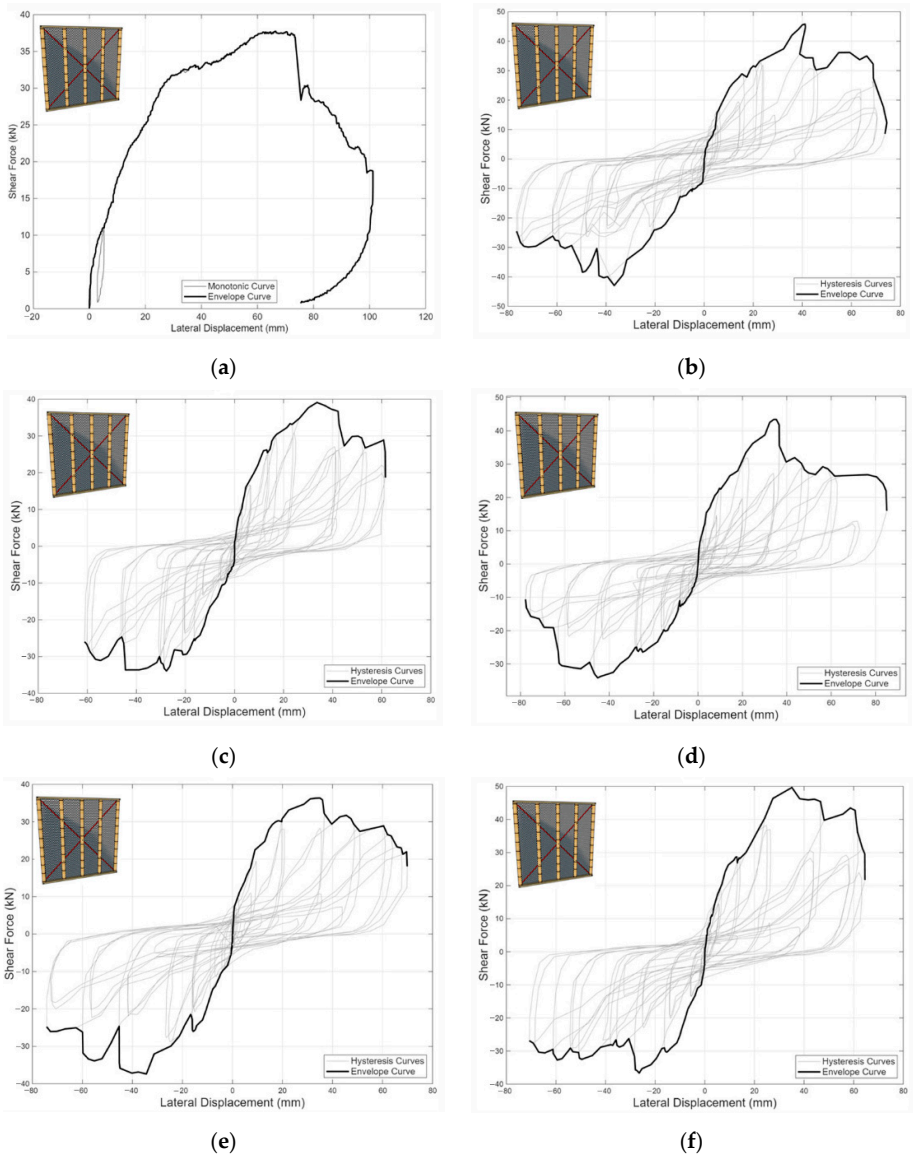

Figure 7. Load–displacement relationships under monotonic and cyclic loading, including corresponding envelope curves for specimens: (**a**) WT1-M-S1; (**b**) WT1-C-S2; (**c**) WT1-C-S3; (**d**) WT1-C-S4; (**e**) WT1-C-S5; (**f**) WT1-C-S6.

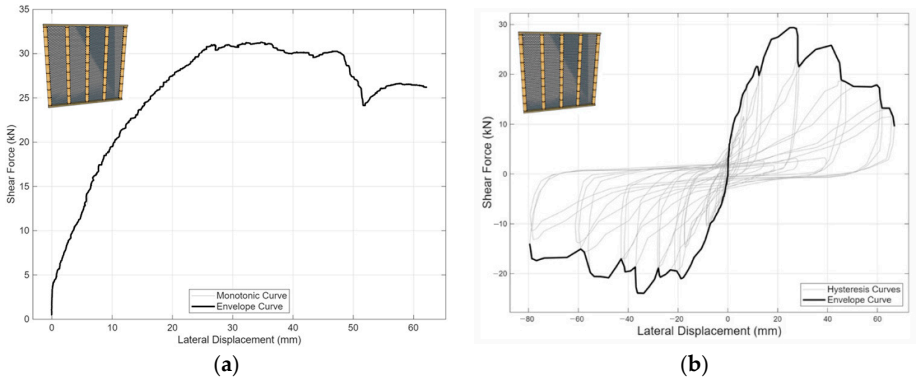

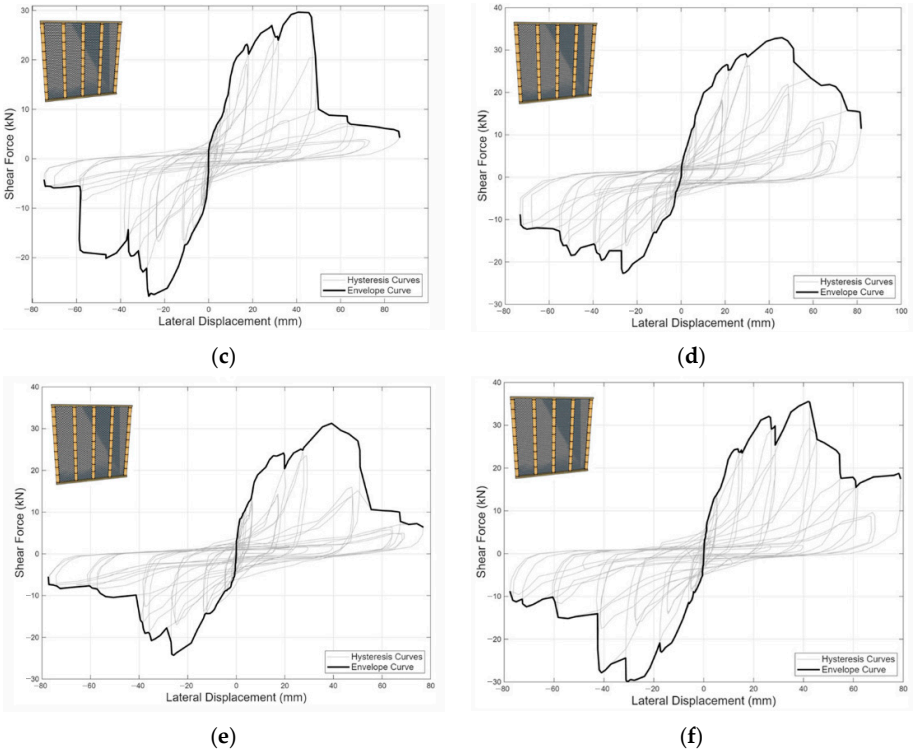

Figure 8. Load–displacement relationships under monotonic and cyclic loading, including corresponding envelope curves for specimens: (**a**) WT2-M-S7; (**b**) WT2-C-S8; (**c**) WT2-C-S9; (**d**) WT2-C-S10; (**e**) WT2-C-S11; (**f**) WT2-C-S12.

Figures 7b–f and 8b–f present the hysteretic responses of WT1 and WT2 under reversed cyclic loading. The derived enveloped curves revealed pronounced asymmetry: lateral resistance in the initial loading direction was consistently higher than in the reversed direction. This asymmetric behavior stems from progressive yielding and partial withdrawal of the nail connectors, which reduced effective stiffness in subsequent cycles.

The load-transfer mechanism in the CBSW panels can be interpreted based on the observed deformation patterns and damage progression. Under lateral loading, the applied force is transferred from the loading beam to the top timber plate and then distributed to the vertical bamboo studs. The load is subsequently transferred to the foundation through the bottom timber plate and the embedded rebar connections.

The overturning of the wall is restrained by the embedded rebar connections at the end studs (B1 and B5), supplemented by hold-down connections provided in the test setup to ensure that uplift is prevented and that the wall response is governed by shear. Sliding is restrained by the embedded rebar connection at the immediate stud (B3). As the frame deforms in shear, the flat bar cross-bracing (when present) and the cement-based mortar cladding restrain overall deformation. As a result, deformation is concentrated at the cladding-to-framing nailed connection.

Typical failure mechanisms are shown in Figure 9 for WT1. Under monotonic loading, damage initiated with simultaneous buckling of the flat bar cross-bracing and yielding of connecting bolts on the compression side, accompanied by nail yielding at the cladding–frame interface. This caused cladding rotation, mortar crushing at the upper and lower compression corners, surface mortar cracking, and chipping. Further loading led to progressive nail withdrawal from the bamboo and nail detachment from the rib lath, particularly along the perimeter and corners, resulting in partial cladding detachment. In several cases, the rib lath tore, causing the nails to detach completely from the mortar

cladding. Nails in mortar-filled bamboo studs showed pronounced yielding due to restricted movement, whereas those in unfilled studs remained relatively straight. Bamboo splitting occurred along intermediate studs, typically near maximum load.

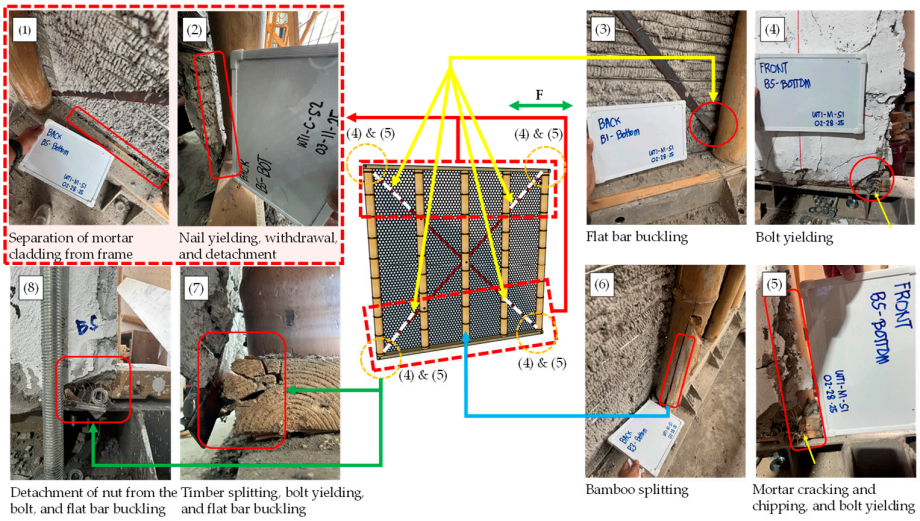

Figure 9. Damage modes for WT1.

Under cyclic loading, WT1 damage progression resembled the monotonic case but was worsened by load reversals. Flat bar buckling and bolt yielding appeared on both sides, nearly simultaneously, while the cladding exhibited rocking motion linked to nail yielding. Mortar cracking and chipping were widespread at corners and timber plate interfaces. Combined bolt yielding and flat bar buckling pushed the cladding outward, accelerating nail withdrawal. In one specimen (WT1-C-S5), the bottom bolt nut detached under excessive tension. Bamboo splitting was observed in some specimens, but it was not dominant and appeared only at or near the maximum load in the monotonic test.

Figure 10 illustrates a typical failure in WT2. Under monotonic loading, the absence of cross-bracing and bolts shifted primary damage to nail connections. Damage began with nail yielding, especially at corners, allowing cladding rotation relative to the frame. Continued rotation caused widespread nail withdrawal from the bamboo, nail detachment from the rib lath, and cladding detachment. In several cases, the rib lath tore like what happened in WT1, causing the nails to detach completely from the mortar cladding. Mortar cracking and chipping occurred at corners, though generally less severe than in WT1 due to the absence of stress induced by cross-bracing.

Under cyclic loading, WT2 damage followed a similar pattern but intensified with load reversals. Nail yielding, withdrawal, and detachment were frequent along the perimeter, particularly near corners, as the cladding rocked. Repeated cycles of loading and unloading caused the nails to progressively loosen, detach, and reinsert during reloading, which ultimately led to permanent cladding separation. Bamboo splitting was limited to one specimen (WT2-C-S11) and remained localized near maximum load.

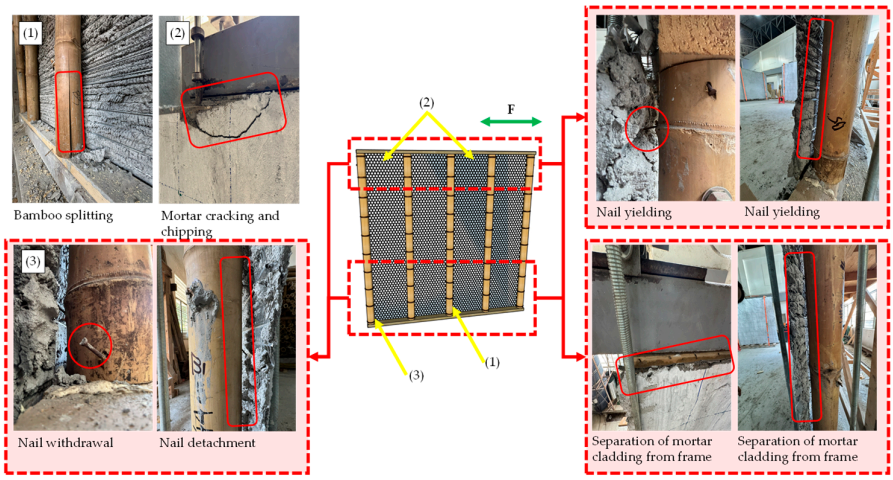

Figure 10. Damage modes for WT2.

Table 3 summarizes the observed damage modes across all specimens. Blue-filled symbols indicate modes first evident at the yield point, while red-filled symbols highlight those prominent at the ultimate point. Black-filled symbols represent damage modes that were observed during testing but were not prevalent at either the yield or ultimate points. Conversely, blank cells denote modes that were not observed at any stage of testing.

Table 3. Damage modes: (a) nail yielding; (b) nail withdrawal from bamboo; (c) nail detachment from rib lath; (d) flat bar buckling; (e) bolt yielding; (f) bamboo splitting; (g) timber splitting; (h) mortar cracking; (i) mortar chipping; (j) separation of mortar cladding from the frame; (k) detachment of nut from the bolt, where blue and red infill indicate damage at yield and ultimate points, respectively.

Wall ID	Damage Modes										
	a	b	c	d	e	f	g	h	i	j	k
WT1-M-S1	●	●	●	●	●	●		●	●	●	
WT1-C-S2	●	●	●	●	●			●	●	●	
WT1-C-S3	●	●	●	●	●	●		●	●	●	
WT1-C-S4	●	●	●	●	●			●	●	●	
WT1-C-S5	●	●	●	●	●		●	●	●	●	●
WT1-C-S6	●	●	●	●	●	●	●	●	●	●	
WT2-M-S7	●	●	●					●	●	●	
WT2-C-S8	●	●	●					●	●	●	
WT2-C-S9	●	●	●					●	●	●	
WT2-C-S10	●	●	●					●	●	●	
WT2-C-S11	●	●	●			●		●	●	●	
WT2-C-S12	●	●	●					●	●	●	

The observed damage modes in the tested CBSW panels, primarily nail yielding, nail withdrawal, and separation of the mortar cladding from the bamboo–timber frame, closely resemble the failure patterns commonly reported in conventional light-frame timber (LFT) shear walls. In LFT shear walls, the cladding-to-framing connections, typically nails or screws, govern lateral capacity, stiffness, ductility, and energy dissipation, with fastener yielding and withdrawal controlling the response under cyclic loading [36–38]. Similarly, in CBSW panels, the overall response is largely governed by the behavior of the nailed cladding-to-framing connections.

Based on the observed damage progression, the behavior of CBSW panels can be described in three main categories. First, damage at the yield point is associated with the

yielding of the cladding-to-framing nailed connections, where most of the deformation and energy dissipation occurs. In the braced configuration (WT1), yielding of the flat bar cross-bracings and connecting bolts was also observed, indicating that the bracing provides an additional load path within the system.

Second, damage at failure is characterized by the gradual separation of the mortar cladding from the frame. This occurs due to nail withdrawal and detachment from the rib lath matrix, which leads to loss of interaction between the cladding and the frame.

Third, isolated damage, such as localized bamboo splitting, was observed only in limited cases (in WT1 under monotonic loading) and did not control the overall response of the wall.

In comparison with conventional LFT shear walls, the overall damage progression and behavior are largely similar, confirming that the response is primarily governed by the cladding-to-framing connections. These results indicate that the shear performance of CBSW panels depends mainly on the behavior of the nailed connections and the integrity of the cladding–frame interface. Therefore, connection detailing, nail distribution, and the quality of the interface are critical factors in controlling stiffness, strength, and ductility. Further research is needed to quantify these effects and support the development of design recommendations for CBSW systems.

3.2. Structural Performance Parameters

Key parameters were derived from the envelope curves of both monotonic and cyclic tests, following the procedures in ISO/TR 21141:2022 [32], which consolidates relevant methods from European, North American, and East Asian standards. These parameters characterize the seismic performance of the CBSW panels, including yield and ultimate forces (F_y and F_u) and corresponding displacements (V_y and V_u), elastic stiffness (K_e), ductility (μ), dissipated energy (E_D), equivalent viscous damping ratio (ζ_{eq}), and stiffness degradation. The shear behavior of the panels under lateral loading was evaluated using the envelope curves shown in Figures 7 and 8. Both WT1 and WT2 exhibited nonlinear behavior from the onset, with no distinct linear–elastic region, a characteristic of light-frame and composite systems with multiple nailed connections where early local slip and localized yielding occur. Consequently, yield points could not be identified visually and required standardized procedures per ISO/TR 21141:2022 [32]. Table 4 summarizes the results.

Table 4. Summary of CBSW shear wall panel test results.

Wall ID	F_{max} (kN)	V_{max} (mm)	F_u (kN)	V_u (mm)	F_y (kN)		V_y (mm)		K_e (kN/mm)		μ	
					F_y	$F_{y,eeep}$	V_y	$V_{y,eeep}$	K_e	K_{eeep}	μ	μ_{eeep}
WT1-M-S1	37.75	66.48	36.94	73.43	25.34	33.49	20.36	18.88	1.41	1.77	3.61	3.89
WT1-C-S2 (+)	45.80	41.13	36.64	39.18	23.74	33.92	10.04	12.63	2.46	2.69	3.90	3.10
WT1-C-S2 (−)	42.93	36.68	34.34	51.29	29.27	36.34	24.27	25.13	1.10	1.45	2.11	2.04
WT1-C-S3 (+)	39.11	33.61	31.29	43.30	21.20	32.88	8.86	9.48	3.08	3.47	4.89	4.57
WT1-C-S3 (−)	33.92	27.72	27.14	45.10	24.40	30.78	14.44	15.51	1.49	1.98	3.12	2.91
WT1-C-S4 (+)	43.40	35.31	34.72	37.15	20.56	33.87	7.58	10.88	2.52	3.11	4.90	3.41
WT1-C-S4 (−)	34.16	45.22	27.33	62.90	21.75	29.76	16.99	19.58	1.20	1.52	3.70	3.21
WT1-C-S5 (+)	36.35	34.95	29.08	48.84	21.66	31.65	8.69	11.15	2.30	2.84	5.62	4.38
WT1-C-S5 (−)	37.38	34.44	29.90	45.30	26.22	32.56	20.46	17.39	1.46	1.87	2.21	2.60
WT1-C-S6 (+)	49.66	35.10	39.73	61.02	25.31	41.72	8.87	13.78	2.55	3.03	6.88	4.43
WT1-C-S6 (−)	36.67	26.47	29.34	29.32	25.88	31.83	10.37	10.77	2.27	2.96	2.83	2.72
Average [1]:	**39.74**	**37.92**	**32.40**	**48.80**	**24.12**	**33.53**	**13.72**	**15.02**	**1.99**	**2.43**	**3.98**	**3.39**
Standard Deviation [1]:	**5.05**	**10.82**	**4.28**	**12.75**	**2.65**	**3.24**	**5.89**	**4.82**	**0.67**	**0.72**	**1.47**	**0.83**

Coefficient of Variation [1]:	**0.13**	**0.29**	**0.13**	**0.26**	**0.11**	**0.10**	**0.43**	**0.32**	**0.34**	**0.30**	**0.37**	**0.25**
WT2-M-S7	31.30	34.69	25.04	51.44	18.55	28.72	8.99	12.09	1.80	2.38	5.72	4.26
WT2-C-S8 (+)	29.40	26.43	23.52	28.03	14.39	24.86	5.23	7.41	2.59	3.35	5.36	3.78
WT2-C-S8 (−)	23.93	33.75	19.14	37.14	18.36	20.72	14.98	13.67	1.30	1.52	2.48	2.72
WT2-C-S9 (+)	29.63	40.75	23.70	47.84	25.15	26.97	23.38	18.08	1.19	1.49	2.05	2.65
WT2-C-S9 (−)	27.78	27.15	22.22	28.19	11.42	22.50	3.10	5.59	3.10	4.03	9.10	5.05
WT2-C-S10 (+)	32.93	45.81	26.34	53.00	21.03	28.78	12.90	13.49	1.73	2.13	4.11	3.93
WT2-C-S10 (−)	22.67	26.49	18.14	37.36	11.89	17.86	10.13	10.93	1.58	1.63	3.69	3.42
WT2-C-S11 (+)	31.28	39.24	25.02	50.82	20.16	26.57	11.03	11.16	1.80	2.38	4.61	4.56
WT2-C-S11 (−)	24.31	25.80	19.45	27.72	11.34	20.22	7.25	11.52	1.41	1.75	3.82	2.41
WT2-C-S12 (+)	35.53	41.84	28.42	44.95	21.70	29.82	9.70	11.71	2.11	2.55	4.63	3.84
WT2-C-S12 (−)	29.99	30.65	23.99	42.29	19.48	26.28	11.61	13.97	1.48	1.88	3.64	3.03
Average [1]:	**28.98**	**33.87**	**23.18**	**40.80**	**17.59**	**24.84**	**10.75**	**11.78**	**1.83**	**2.28**	**4.47**	**3.60**
Standard Deviation [1]:	**3.99**	**7.17**	**3.19**	**9.75**	**4.66**	**3.97**	**5.37**	**3.31**	**0.58**	**0.80**	**1.88**	**0.84**
Coefficient of Variation [1]:	**0.14**	**0.21**	**0.14**	**0.24**	**0.27**	**0.16**	**0.50**	**0.28**	**0.32**	**0.35**	**0.42**	**0.23**

[1] Bold values represent the calculated average, standard deviation, and coefficient of variation (COV) for each wall configuration.

3.2.1. Yield and Ultimate Loads and Displacements

The yield and ultimate loads of WT1 ranged approximately from 20.56 kN to 26.22 kN and 27.14 kN to 39.73 kN, respectively, with an average yield displacement of 13.72 mm. For WT2, the yield and ultimate loads were lower, ranging approximately from 11.34 kN to 25.15 kN and 18.14 kN to 28.42 kN, respectively, with an average yield displacement of 17.59 mm. Compared with WT2, the addition of flat bar cross-bracing in WT1 substantially enhanced bearing capacity, increasing yield and ultimate loads by approximately 35–40%. Across all specimens, yield loads (F_y) were approximately 40–80% of the F_{max}, while yield displacements (V_y) were 20–70% of the V_{max}.

The EEEP method was selected because it consistently provides higher estimates for yield load ($F_{y,eeep}$) compared to the JIS A 1414-2:2010 [33] method. This is advantageous for strength-based design, as it allows for a more efficient use of the wall's actual capacity. Higher yield values arise because the EEEP method is based on the work–energy principle. Instead of identifying yield based only on initial stiffness, EEEP creates an equivalent bilinear curve that matches the total energy under the actual envelope up to V_u, resulting in a yield point that lies farther from the origin, as observed in the load–displacement responses. While the EEEP method produces a higher yield load ($F_{y,eeep}$) and yield displacement ($V_{y,eeep}$), the larger $V_{y,eeep}$ increases the denominator in the ductility ratio ($\mu_{eeep} = V_u/V_{y,eeep}$). This effect tends to produce lower ductility values when the EEEP method is used compared to the method [33] that identifies yield at an earlier stage of the response.

3.2.2. Lateral Stiffness

The computed stiffness values for each panel are presented in Table 4. WT1 exhibited higher stiffness than WT2, approximately 9% greater in K_e and 6% greater in K_{eeep}. This increase is attributed to the flat bar cross-bracing in WT1, which provided additional lateral restraint and load sharing between frame and mortar cladding. Cross-bracing limits relative displacement between vertical and horizontal frame members, thereby enhancing initial in-plane rigidity. In contrast, the absence of cross-bracing in WT2 resulted in greater frame flexibility, with lateral resistance relying primarily on nail connections. Although

the stiffness difference is moderate, WT1 demonstrated a stiffer early-stage response and better resistance to initial lateral deformation.

Comparison of the two stiffness measures also reveals insight into elastic behavior. In both configurations, K_{eeep} was found to be approximately 1.2 times higher than K_e. This is expected because K_{eeep} is defined by a line drawn from the origin to $0.4F_{max}$, thereby encompassing part of the initial, steeper region of the envelope curve. In contrast, K_e is evaluated over a range that already includes minor nonlinearity due to local slip and connection yielding. Thus, a higher K_{eeep} value indicates that the system exhibits an initially stiffer response before local deformations become significant.

3.2.3. Ductility

Ductility factors for each panel are summarized in Table 4. WT2 exhibited greater ductility than WT1. This is expected, as the absence of flat bar cross-bracing in WT2 allowed freer frame deformation under lateral loading, resulting in larger inelastic displacements. In contrast, cross-bracing in WT1 increased stiffness and strength but constrained deformation, leading to relatively lower ductility.

When comparing the two ductility parameters, the values of μ were consistently higher than those of μ_{eeep}. This difference can be attributed to the way the yield point is defined in each method. In the conventional method [33], the yield point (V_y) is obtained directly from the experimental load–displacement curve, where it typically occurs at a smaller displacement closer to the origin. In contrast, the EEEP yield point ($V_{y,eeep}$) is determined from the intersection of the bilinear idealization of the curve, which lies farther from the origin because it accounts for energy equivalence rather than instantaneous slope change. Consequently, the EEEP method provides a more conservative estimate of ductility, as it reflects an average or smooth representation of the wall's elastic–plastic transition rather than a localized yield response.

Although both methods are valid, the EEEP method is recommended for design purposes in this study. It provides a more conservative (lower) ductility value, which is advantageous for safe estimation of seismic displacement demands in performance-based design. The slightly higher yield strength estimate from EEEP also aligns better with a safe, strength-based verification of capacity.

3.2.4. Energy Dissipation

Figure 11 presents the cumulative dissipated energy for WT1 and WT2. Dissipated energy increases with cycle number during the initial stages, reflecting progressive activation of inelastic mechanisms such as nail yielding, nail withdrawal, and rotation of the mortar cladding.

Overall, WT1 consistently dissipated more energy than WT2. This is attributed to the flat bar cross-bracing in WT1, which stabilized the frame, delayed excessive distortion, and enabled the panel to mobilize greater inelastic deformation capacity. Cross-bracing also prevented premature loss of resistance in the nailed connections, supporting larger, more stable hysteresis loops and higher energy dissipation over the test duration. In contrast, WT2 lacks this cross-bracing, causing deformation to concentrate more directly on the nail, bamboo, and mortar cladding interface. This results in earlier withdrawal or localized failure of connections, diminishing the effective energy dissipation capacity of the wall panel.

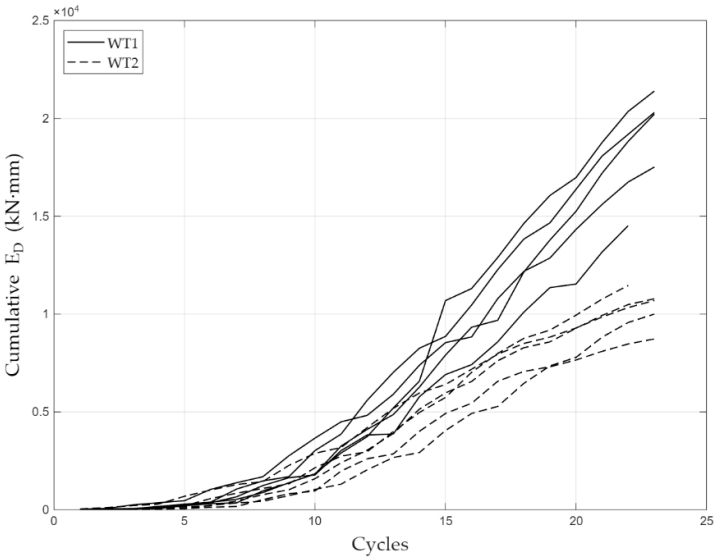

Figure 11. Cumulative E_D for WT1 and WT2.

A similar trend appears in the equivalent viscous damping ratios as presented in Table 5. WT1 generally attains higher ζ_{eq} values than WT2 throughout testing. The improved damping performance of WT1 reflects its ability to maintain stable hysteresis loops, retain strength across cycles, and distribute energy dissipation mechanisms more effectively. WT2, being more flexible but less restrained, produced narrower hysteresis loops and lower capacity to convert input energy into stable inelastic deformation, resulting in reduced damping overall.

Table 5. The equivalent viscous damping ratio of the wall panels.

WALL ID	Cycle					
	8	**11**	**14**	**17**	**20**	**23**
WT1-C-S2	0.16	0.37	0.95	1.01	0.19	0.22
WT1-C-S3	0.23	0.19	0.19	0.18	0.15	0.16
WT1-C-S4	0.19	0.20	0.25	0.25	0.25	0.26
WT1-C-S5	0.36	0.27	0.27	0.20	0.28	0.25
WT1-C-S6	0.22	0.26	0.18	0.20	0.16	0.17
Average [1]:	**0.23**	**0.26**	**0.37**	**0.37**	**0.21**	**0.21**
WT2-C-S8	0.17	0.15	0.17	0.17	0.20	0.18
WT2-C-S9	0.36	0.23	0.24	0.25	0.29	0.23
WT2-C-S10	0.17	0.18	0.20	0.24	0.23	0.20
WT2-C-S11	0.24	0.32	0.27	0.29	0.19	0.24
WT2-C-S12	0.24	0.22	0.22	0.25	0.15	0.13
Average [1]:	**0.24**	**0.22**	**0.22**	**0.24**	**0.21**	**0.19**

[1] Bold values represent the calculated average for each wall configuration.

Taken together, the higher dissipated energy (E_D) and equivalent viscous damping ratios (ζ_{eq}) in WT1 confirms that flat bar cross-bracing significantly enhances energy absorption and seismic performance of CBSW panels compared with WT2.

Table 6 compares the cycle-specific equivalent viscous damping ratios (ζ_{eq}) from this study with values reported in the literature. Because previous studies report damping either at discrete points (elastic, yield, peak, failure) or fixed drift levels rather than cycle numbers, direct comparison requires approximate mapping of deformation stages (see Notes column). Overall, the CBSW panels exhibit damping values within or slightly above

the ranges reported, particularly at later degradation stages (Cycles 14–20), suggesting potential favorable energy dissipation capacity under repeated loading.

Table 6. Comparison of equivalent viscous damping ratios between current CBSW panels and values from existing literature.

Reference	Wall Description	ζ_{eq} Values or Range	Notes
[39]	80 cm × 90 cm timber frame with 3 vertical posts, 2 horizontal members, reinforced with glass fiber-reinforced polymer (GFRP) at the connections, and with brick masonry infill.	At 1% drift: 0.10–0.19	
[13]	2.2 m × 2.2 m frame with 3 vertical timber elements, 2 diagonal timber braces, with two wooden sill beams, sheathed with *Guadua* bamboo strips, and with the wall infilled with a mixture of soil and fiber.	At 1% drift: 0.15	Drift-based. 1% drift aligns with Cycle 14 in this study, which is at or near F_{max} (≈0.37 for WT1 and 0.22 for WT2).
[13]	2.2 m × 2.2 m frame with 3 vertical *Guadua* elements, 2 diagonal *Guadua* braces, with two wooden sill beams, sheathed with *Guadua* bamboo strips, and with the wall infilled with a mixture of soil and natural fiber.	At 1% drift: 0.11	
[9]	2.49 m × 3.0 m Moso bamboo frame with bamboo split K-shaped brace sheathed with gypsum-based mortar.	At elastic point: 0.146 At yield point: 0.154 At peak point: 0.118 At failure point: 0.132	Point-based. Approximate alignment: Yield point is at Cycles 6–8 (≈0.23 for WT1 and 0.24 for WT2), peak point ≈ Cycle 14 (≈0.37 for WT1 and 0.22 for WT2), and failure point ≈ Cycle 20 (≈0.21 for both WT1 and WT2).
[9]	3.0 m × 3.0 m Moso bamboo frame with bamboo split X-shaped brace sheathed with gypsum-based mortar.	At elastic point: 0.186 At yield point: 0.20 At peak point: 0.168 At failure point: 0.136	
Present Study	2.4 m × 2.4 m bamboo–timber frame with 5 vertical bamboo studs, 2 timber horizontal plates, with flat bar cross-bracing, and sheathed with 25 mm mortar plaster.	At Cycle 8: 0.23 At Cycle 14: 0.37 At Cycle 20: 0.21	Cycle-based (3rd repetition). Range: 0.21–0.23 for WT1 and 0.21–0.24 for WT2.
Present Study	2.4 m × 2.4 m bamboo–timber frame with 5 vertical bamboo studs, 2 timber horizontal plates, and sheathed with 25 mm mortar plaster.	At Cycle 8: 0.24 At Cycle 14: 0.22 At Cycle 20: 0.21	

3.2.5. Stiffness Degradation

Both wall configurations exhibit a clear decreasing trend in secant stiffness as cyclic loading progresses, as shown in Figure 12. The initial degradation is notably steep, indicating that the panels lack a well-defined linear–elastic phase. Instead, nonlinear behavior develops at an early stage of loading due to localized deformations at the interface between the cladding and framing. This rapid early-stage loss of stiffness is driven by the progressive yielding and withdrawal of nail fasteners, and the gradual loosening of the cladding-to-framing nailed connection. The specific behavior of the nail fasteners varies by location; in unfilled bamboo regions, nails tend to withdraw gradually, whereas in mortar-filled regions, the added confinement forces the nails into plastic-bending. Because these micro-failures initiate at different locations and stages throughout the wall, they

produce a state of distributed inelasticity that results in the rapid stiffness loss observed in the test data.

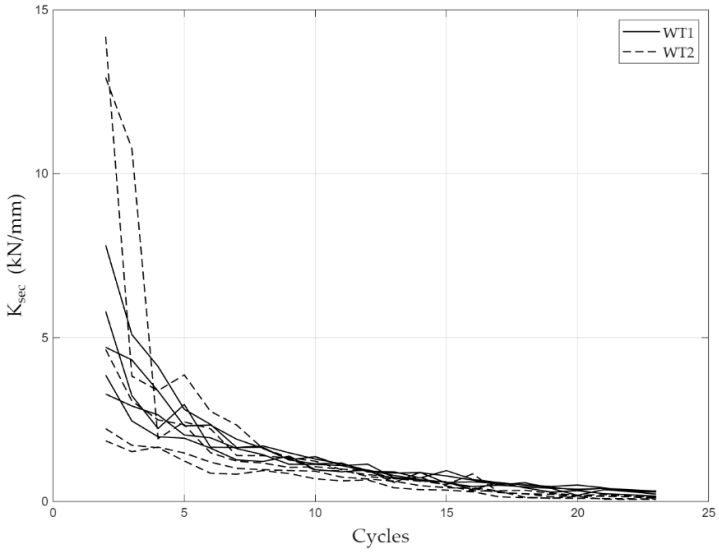

Figure 12. Stiffness degradation (K_{sec}) for WT1 and WT2.

As loading continued toward the yield point, the degradation rate decreased, indicating a transition from localized damage to a more stable load-resisting configuration. At this stage, the remaining effective fasteners and intact cladding regions contribute more uniformly to load transfer. Beyond peak load, stiffness degradation becomes gradual, suggesting that the dominant damage mechanisms—primarily nail yielding—have already been established, and further deformation is governed by continued connection slip rather than the formation of new damage modes.

A comparison between WT1 and WT2 shows that the latter experiences a noticeably steeper stiffness degradation, especially in the early cycles. This behavior is attributed to the absence of flat bar cross-bracing in WT2, resulting in a single load-transfer mechanism between the mortar cladding and the frame dominated by nailed connections. In contrast, WT1 benefits from an additional load path provided by the flat bar cross-bracing, which contributes to force redistribution and delays early stiffness loss. However, as loading increases and the bracing yields or buckles, the structural response of WT1 transitions toward a nail connection-dominated mechanism similar to WT2.

These observations indicate that the lateral stiffness of CBSW is highly dependent on the integrity and performance of nailed connections. The observed rapid initial stiffness degradation indicates that serviceability performance in CBSW panels is governed by connection deformation, particularly nail yielding and withdrawal, rather than by the failure of the primary structural material. Consequently, the nailed cladding-to-frame connection plays a critical role in controlling stiffness and should be a key focus in design and detailing.

3.3. Shear Strength and Shear Capacity

For the present dataset, a sampling factor of 1.9 was applied in accordance with ISO 12122-6:2017 [35]. The characteristic shear strength of WT1 panels was determined as 31.66 kN, approximately 48% higher than that of WT2 panels (21.43 kN). Correspondingly, the characteristic shear capacity reached 13.19 kN/m for WT1 and 8.93 kN/m for WT2.

An alternative set of characteristic values can be proposed using the yield load from the EEEP idealization ($F_{y,eeep}$). This approach is motivated by the observation that

standard deviations are consistently lower at $F_{y,eeep}$ ($SD = 3.09$ for WT1 and 3.78 for WT2) compared to the values recorded at the F_{max} ($SD = 4.81$ for WT1 and 3.81 for WT2). The reduced scatter leads to more statistically stable and reliable characteristic estimates after applying the ISO 12122-06:2017 [35] sampling factor. Adopting $F_{y,eeep}$ for characteristic strength estimation provides a more robust basis for design, particularly in systems like composite bamboo shear walls that exhibit gradual yielding and where variability at peak load can reduce confidence in the 5th percentile values.

For WT1 panels, the $F_{y,eeep}$-based characteristic shear strength is 29.28 kN, which is approximately 7.5% lower than the F_{max}-based value but benefits from reduced scatter (3.09% SD vs. 4.81% SD at F_{max}). Similarly, for WT2, $F_{y,eeep}$-based characteristic shear strength is 17.83 kN. The corresponding characteristic shear capacities are 12.20 kN/m for WT1 and 7.43 kN/m for WT2. The characteristic shear capacity values serve as the primary design input for the simplified structural analysis of CBSW systems, consistent with the methodology outlined in the Philippine Guidelines on Bamboo Design and Construction 2025 [40] and international frameworks, such as Colombian NSR-10 Título G—Estructuras de Madera y Estructuras de Guadua [41]. In these standards, the structural adequacy of a building is ensured by providing the cumulative length of walls whose total characteristic resistance meets the lateral demand. By establishing these fundamental design parameters, this study enables the transition from laboratory testing to code-compliant construction.

4. Conclusions

This experimental study characterized the shear performance and damage behavior of full-scale composite bamboo shear wall (CBSW) panels under monotonic and cyclic loading, compared with and without flat bar cross-bracing. The braced panels (WT1) consistently exhibited higher lateral strength and initial stiffness, with characteristic shear strength and capacity approximately 48% higher than the unbraced panels (WT2), demonstrating the cross-bracing's effective contribution to load distribution and delayed localized failure. In contrast, WT2 panels showed greater ductility, allowing more distributed deformation through progressive nail yielding and withdrawal. Both configurations displayed gradual load deterioration after peak strength, while the EEEP method yielded higher and more conservative estimates of yield load and displacement compared to the JIS A 1414-2:2010 approach.

These findings establish the first formal experimental baseline for CBSW systems using the ISO 21581:2010 (E) Method I protocol, providing the scientific evidence necessary to transition this technology from traditional practice to an engineered, code-compliant solution. This study fundamentally affirms the consistency of CBSW with established light-frame timber (LFT) principles—a behavior previously assumed but not empirically verified—while quantifying the specific mechanical trade-offs between strength and ductility introduced by the inclusion of flat bar cross-bracing.

The results confirm that CBSW panels, particularly when reinforced with cross-bracing, offer a viable low-carbon alternative for lateral load resistance in low-rise structures in seismic-prone regions. The inclusion of timber plates and mortar cladding effectively mitigates bamboo's geometric and durability limitations, while the nailed connections provide the primary source of ductility and energy dissipation.

As an alternative for practical design, characteristic shear strength and capacity values can also be proposed based on $F_{y,eeep}$. This approach provides a more robust and statistically stable basis, benefiting from consistently lower standard deviation at the yield point and offering reliable estimates well suited to the gradual yielding behavior observed in CBSW panels.

Nevertheless, an important research gap remains. The present work focuses on individual panel behavior; further studies are needed to evaluate the interaction and load-

sharing in multi-panel systems, where the collective structural response is influenced by the redundancy of the full assembly. There is also a critical need to develop and validate high-fidelity numerical models that can accurately simulate the lateral response observed in this study. Such models would allow for broader parametric investigations and the optimization of CBSW configurations without the need for exhaustive full-scale testing. Standardized design value and partial safety factors tailored specifically to CBSW systems are also lacking, and the current reliance on timber-oriented standards may require validation or adaptation for bamboo–mortar composites. Addressing these gaps will be essential to support the safe, code-compliant, and widespread adoption of CBSW as a sustainable solution for disaster-resilient socialized housing.

Author Contributions: Conceptualization, M.J.C.A., M.C.F., and N.P.N.P.; methodology, M.J.C.A. and N.P.N.P.; software, M.J.C.A. and N.P.N.P.; validation, M.J.C.A., M.C.F., L.E.O.G., L.F.L., and N.P.N.P.; formal analysis, M.J.C.A., M.C.F., and N.P.N.P.; investigation, M.J.C.A., M.C.F., and N.P.N.P.; resources, L.E.O.G., L.F.L., and N.P.N.P.; data curation, M.J.C.A., M.C.F., and N.P.N.P.; writing—original draft preparation, M.J.C.A., M.C.F., and N.P.N.P.; writing—review and editing, L.E.O.G., L.F.L., and N.P.N.P.; visualization, M.J.C.A.; supervision, L.E.O.G., L.F.L., and N.P.N.P.; project administration, L.E.O.G., L.F.L., and N.P.N.P.; funding acquisition, L.E.O.G., L.F.L., and N.P.N.P. All authors have read and agreed to the published version of the manuscript.

Funding: This research was funded by the Hilti Foundation.

Data Availability Statement: The original contributions presented in the study are included in the article, further inquiries can be directed to the corresponding author.

Acknowledgments: The authors would like to thank the Department of Science and Technology—Engineering Research and Development for Technology for providing support. Special thanks are also extended to the BSCE students of the Technological University of the Philippines—Manila for their valuable assistance in the fabrication and testing of the wall specimens.

Conflicts of Interest: All authors declare no conflict of interest.

References

1. UN-Habitat Philippines. *UN-Habitat Philippines Country Report 2023*; UN-Habitat Philippines: Mandaluyong City, Philippines, 2023; p. 32.
2. Internal Displacement Monitoring Centre. *Global Report on Internal Displacement 2021*; Internal Displacement Monitoring Centre: Genève, Switzerland, 2021.
3. Di Gangi, G.; Demartino, C.; Quaranta, G. Bamboo Lightweight Shear Walls: Modeling and Identification of Sheathing-to-Framing Connections for Seismic Response Analysis. *Int. J. Struct. Glass Adv. Mater. Res.* **2020**, *4*, 149–159. https://doi.org/10.3844/sgamrsp.2020.149.159.
4. Adier, M.F.V.; Sevilla, M.E.P.; Valerio, D.N.R.; Ongpeng, J.M.C. Bamboo as Sustainable Building Materials: A Systematic Review of Properties, Treatment Methods, and Standards. *Buildings* **2023**, *13*, 2449. https://doi.org/10.3390/buildings13102449.
5. Chen, M.; Ye, L.; Li, H.; Wang, G.; Chen, Q.; Fang, C.; Dai, C.; Fei, B. Flexural Strength and Ductility of Moso Bamboo. *Constr. Build. Mater.* **2020**, *246*, 118418. https://doi.org/10.1016/j.conbuildmat.2020.118418.
6. Aniñon, M.J.C.; Garciano, L.E.O. Advances in Connection Techniques for Raw Bamboo Structures—A Review. *Buildings* **2024**, *14*, 1126. https://doi.org/10.3390/buildings14041126.
7. Muhammad, N.A.G.; Orejudos, J.N.; Aniñon, M.J.C. A Compendium of Research, Tools, Structural Analysis, and Design for Bamboo Structures. *Buildings* **2024**, *14*, 2419. https://doi.org/10.3390/buildings14082419.
8. Ahmad, Z.; Upadhyay, A.; Ding, Y.; Emamverdian, A.; Shahzad, A. Bamboo: Origin, Habitat, Distributions and Global Prospective. In *Biotechnological Advances in Bamboo*; Ahmad, Z., Ding, Y., Shahzad, A., Eds.; Springer Singapore: Singapore, 2021; pp. 1–31. ISBN 978-981-16-1309-8.
9. Kou, Y.; Xu, G.; Ren, Q.; Hao, J.; Tian, L. Experimental Investigations into the Cyclic Performance of Innovative Original Bamboo Frame and Gypsum-Based Mortar Composite Walls. *Structures* **2025**, *80*, 109890. https://doi.org/10.1016/j.istruc.2025.109890.

10. Kaminski, S.; Trujillo, D.; Lopez, L.F. Preliminary Strengths, Stiffness, and Ductilities for Various Composite Bamboo Shear Wall Systems. In Proceedings of the World Conference on Earthquake Engineering WCEE 2024, Milan, Italy, 30 July 2024.
11. Kaminski, S.; Lawrence, A.; Trujillo, D. *Design Guide for Engineered Bahareque Housing*; International Network for Bamboo and Rattan (INBAR): Beijing, China, 2016.
12. Palacios, A.; Angumba, P. Bahareque as a Sustainable Construction System: Analysis of Unit Prices. *IOP Conf. Ser. Mater. Sci. Eng.* **2021**, *1203*, 032118. https://doi.org/10.1088/1757-899X/1203/3/032118.
13. Cristancho, K.; Otálvaro, I.F.; Ruiz, D.M.; Barrera, N.; Villalba-Morales, J.D.; Alvarado, Y.A.; Cundumí, O. Seismic Behavior of Bahareque Walls Under In-Plane Horizontal Loads. *Buildings* **2024**, *15*, 4. https://doi.org/10.3390/buildings15010004.
14. Mite-Anastacio, F.; Tello-Ayala, K.; García-Troncoso, N.; Silva, C.E.; Malaga-Chuquitaype, C.; Arévalo, K.; Villao, D. Structural Behavior of Cemented Bahareque for Social Housing: A Case Study in Guayaquil City, Ecuador. *Front. Built Environ.* **2022**, *8*, 922397. https://doi.org/10.3389/fbuil.2022.922397.
15. Cayme, J.-M. Chemistry of 19th Century Lime Mortar on a Tabique Pampango (Wattle-and-Daub) from the Philippines. *Ge-Conserv.* **2022**, *21*, 55–63. https://doi.org/10.37558/gec.v21i1.1034.
16. Manser, N.; Steiger, R.; Geiser, M.; Otti, M.; Frangi, A. Shear Resistance of Oriented Strand Board Panel Sheathings in Timber-Framed Shear Walls. *Eng. Struct.* **2024**, *316*, 118461. https://doi.org/10.1016/j.engstruct.2024.118461.
17. Branco, J.; Matos, F.; Lourenço, P. Experimental In-Plane Evaluation of Light Timber Walls Panels. *Buildings* **2017**, *7*, 63. https://doi.org/10.3390/buildings7030063.
18. Xiao, Y.; Li, Z.; Wang, R. Lateral Loading Behaviors of Lightweight Wood-Frame Shear Walls with Ply-Bamboo Sheathing Panels. *J. Struct. Eng.* **2015**, *141*, B4014004. https://doi.org/10.1061/(ASCE)ST.1943-541X.0001033.
19. Villalba-Morales, J.D.; Suárez-Reyes, A.; Cristancho, K.; Sánchez, J.A.G.; Otálvaro, I.F.; Cundumi-Sánchez, O.; Ruiz, D.M. Finite Element Modeling of the Structural Response of Bahareque Walls Under Cyclic Loads. *Buildings* **2025**, *15*, 3460. https://doi.org/10.3390/buildings15193460.
20. *ISO 21581:2010 (E)*; Timber Structures—Static and Cyclic Lateral Load Test Methods for Shear Walls. International Organization for Standardization: Geneva, Switzerland, 2010.
21. *ISO 19624:2018*; Bamboo Structures—Grading of Bamboo Culms—Basic Principles and Procedures. International Organization for Standardization: Geneva, Switzerland, 2018.
22. Cacanando, C.J.D.C.; López, L.F.; Atienza, E.; Pradhan, N.P.N. Experimental Characterization of Mechanical Properties of *Bambusa blumeana* Bamboo Poles and Determination of Design Values. *Constr. Build. Mater.* **2024**, *490*, 142498.
23. *BS 4360:1990*; British Standard Specification for Weldable Structural Steels. British Standard Institute British Standard Institute: London, UK, 1990.
24. *ASTM A615/A615M-22*; Standard Specification for Deformed and Plain Carbon-Steel Bars for Concrete Reinforcement. ASTM International ASTM International: West Conshohocken, PA, USA, 2022. https://doi.org/10.1520/A0615_A0615M-22.
25. *ASTM A307-21*; Standard Specification for Carbon Steel Bolts, Studs, and Threaded Rod 60 000 PSI Tensile Strength. ASTM International ASTM International: West Conshohocken, PA, USA, 2021. https://doi.org/10.1520/A0307-21.
26. *A653M-20*; Specification for Steel Sheet, Zinc-Coated (Galvanized) or Zinc-Iron Alloy-Coated (Galvannealed) by the Hot-Dip Process. ASTM International ASTM International: West Conshohocken, PA, USA, 2020. https://doi.org/10.1520/A0653_A0653M-20.
27. *ASTM C1329/C1329M-23*; Standard Specification for Mortar Cement. ASTM International ASTM International: West Conshohocken, PA, USA, 2023. https://doi.org/10.1520/C1329_C1329M-12.
28. *ASTM C109/C109M-21*; Standard Test Method for Compressive Strength of Hydraulic Cement Mortars (Using 2-in. or [50 Mm] Cube Specimens). ASTM International ASTM International: West Conshohocken, PA, USA, 2021. https://doi.org/10.1520/C0109_C0109M-21.
29. *ASTM F1667/F1667M-21a*; Standard Specification for Driven Fasteners: Nails, Spikes, and Staples. ASTM International ASTM International: West Conshohocken, PA, USA, 2021. https://doi.org/10.1520/F1667_F1667M-21A.
30. Bibal, C.B.; Estores, G.B.; López, L.F.; Pradhan, N.P.N. Lateral Overturning Tests of Cement-Bamboo Frame Technology Panels Using ISO 21581 Method II Protocol. *Civ. Eng. Arch.* **2026**, *14*, 486–497. https://doi.org/10.13189/cea.2026.140132.
31. *ASTM E2126-19*; Standard Test Methods for Cyclic (Reversed) Load Test for Shear Resistance of Vertical Elements of the Lateral Force Resisting Systems for Buildings. ASTM International ASTM International: West Conshohocken, PA, USA, 2019. https://doi.org/10.1520/E2126-19.
32. *ISO/TR 21141:2022*; Timber Structures—Timber Connections and Assemblies—Determination of Yield and Ultimate Characteristics and Ductility from Test Data. International Organization for Standardization: Geneva, Switzerland, 2022.

33. *JIS A 1414-2:2010*; Performance Test Methods of Panel Components for Building Construction—Part 2: Tests for Mechanical Properties. Japanese Standards Association: Tokyo, Japan, 2010**.**
34. Azinović, B.; Kržan, M.; Pazlar, T. In-Plane Lateral Testing of Timber Based Shear Walls and the Influence of Loading Rate. In Proceedings of the 1st Croatian Conference on Earthquake Engineering, University of Zagreb Faculty of Civil Engineering, Zagreb, Croatia, 22 March 2021; pp. 961–972.
35. *ISO 12122-6:2017 (E)*; Timber Structures—Determination of Characteristic Values—Part 6: Large Components and Assemblies. International Organization for Standardization: Geneva, Switzerland, 2017**.**
36. Anderson, E.; Leichti, R.; Sutt, E.; Rosowsky, D. Sheathing Nail Bending-Yield Stress: Effect on Cyclic Performance of Wood Shear Walls. *Wood Fiber Sci.* **2007**, *39*, 536–547.
37. Echeverry, J.S.; Correal, J.F. Cyclic Behavior of Laminated Guadua Mat Sheathing-to-Framing Connections. *Constr. Build. Mater.* **2015**, *98*, 69–79. https://doi.org/10.1016/j.conbuildmat.2015.08.109.
38. Liu, M.; Su, N.; Zhu, X. Design and Performance of Nail Connection in Wood Framing Shear Walls. *Wood Res.* **2022**, *67*, 291–301. https://doi.org/10.37763/wr.1336-4561/67.2.291301.
39. Vasconcelos, G.; Poletti, E.; Salavessa, E.; Jesus, A.M.P.; Lourenço, P.B.; Pilaon, P. In-Plane Shear Behaviour of Traditional Timber Walls. *Eng. Struct.* **2013**, *56*, 1028–1048. https://doi.org/10.1016/j.engstruct.2013.05.017.
40. Association of Structural Engineers of the Philippines, Inc.; Base Bahay Foundation, Inc. Association of Structural Engineers of the Philippines, Inc. *Philippine Guidelines on Bamboo Design and Construction 2025*; Base Bahay Foundation: Makati City, Philippines, 2025.
41. *NSR-10*; Título G—Estructuras de Madera y Estructuras de Guadua. Asociación Colombiana de Ingeniería Sísmica: Bogotá, Colombia, 2010.